Available online at www.sciencedirect.com
SCIENCE DIRECT
Journal of Molecular Catalysis A: Chemical 244 (2006) 151–159
JOURNAL OF MOLECULAR CATALYSIS A: CHEMICAL
www.elsevier.com/locate/molcata

Facile synthesis and characterization of ordered mesostructured nickel catalysts

Taewook Kang, Younggeun Park, Jongheop Yi *

School of Chemical and Biological Engineering, Institute of Chemical Processes, Seoul National University, Shinlim-dong, Kwanak-ku, Seoul 151-742, South Korea

Received 17 June 2005; received in revised form 17 June 2005; accepted 7 September 2005
Available online 10 October 2005

Abstract

Nickel precursors were added midway during the self-assembly of a block copolymer and a silica precursor, leading to the rapid and facile production (one-step) of highly ordered mesoporous nickel catalysts. Ni-MH and Ni-MS were prepared using HCl or H_2SO_4 as the acid source. Both Ni-MH and Ni-MS contain uniform mesopore channels with a periodic mesochannel alignment (space group, *p*6*mm*). Ni-MS contained smaller nickel particles than Ni-MH, as evidenced by XRD and TEM analyses. TEM images clearly show that NiO in Ni-MH is deposited along the mesopore channel. Both the critical dependence of the temperature used in the synthesis of Ni-MH on nickel loading and the increase in nickel loading resulting from the use of SO_4^{2-} (Ni-MS) as a counteranion indirectly suggest that the self-assembly of mesostructured nickel catalysts mainly involves an electrostatic pathway and complexation between the polyethylene oxide (PEO) branch in P123 and Ni^{2+}. The routes for the self-assembly appear to largely involve electrostatic interactions in the case of Ni-MS and coordination by PEO in the case of Ni-MH. The morphologies of the Ni-MH and Ni-MS catalysts can be manipulated by varying the reaction temperature used, thus permitting the production of uniform rod-like forms or uniform spherical particles. As the reaction temperature is increased, both Ni-MH and Ni-MS appear to have a more curved shape in both meso and macroscopic views.

Keywords: Nickel precursor; Mesoporous silica; Self-assembly; Mesostructured catalyst; Selective adsorption; Mesochannel; Hydrodechlorination

1. Introduction

Ordered mesoporous materials [1] show a large BET surface area, high porosity, controllable and narrowly distributed pore sizes, and an ordered pore arrangement. These materials are potentially promising candidates for use in catalysts [2–9], adsorbents [10–13], sensors [14], and hosts [15,16] for host-guest encapsulation in composite materials. Among the wide variety of application areas, our interest has focused on the preparation of heterogeneous catalysts supported on ordered mesoporous materials. In such a system, the confinement of nanoparticles in the mesochannels of mesoporous silicas aids in stabilizing the highly dispersed metals and oxides in uniform porous matrixes [7,8,17]. Furthermore, ordered mesoporous materials have a more uniform pore structure and a larger surface area than conventional industrial catalyst supports, and their tunable mesoporosity may reduce the extent of deactivation due to coke formation and plugging phenomenon that occurs in the micropores, which blocks pores, leading to limitations in the mass-transfer of reactants and products. Therefore, ordered mesoporous materials have the potential for use as high performance catalyst supports. Among the diverse ordered mesostructured family, because of its relatively high mechanical, thermal, and hydrothermal stabilities with a well-defined pore structure and uniform pore sizes of cylindrical shape [18,19], we have concluded that SBA-15 is one of the most promising catalyst supports for practical industrial applications in the field of heterogeneous catalysis. In order to develop an effective mesoporous catalyst supported on SBA-15, in a departure from these synthetic methods, we have considered the possibility of the one-step preparation of mesostructured catalysts supported on SBA-15 (Scheme 1, C), which would result in a significant reduction in both cost (increases in the economic feasibility of ordered mesoporous materials) and the time required for the manufacture of mesostructured catalysts. This novel strategy demonstrates that

* Corresponding author. Tel.: +82 2 880 7438; fax: +82 2 888 7295.
E-mail address: jyi@snu.ac.kr (J. Yi).

1381-1169/$ – see front matter © 2005 Elsevier B.V. All rights reserved.
doi:10.1016/j.molcata.2005.09.003

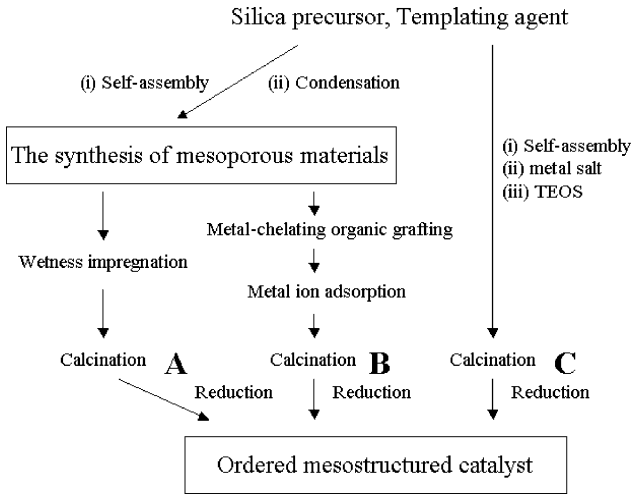

Scheme 1. The preparation method of mesostructured catalysts using: (A) conventional technique (wetness impregnation); (B) adsorption-mediating method; and (C) one-step procedure.

mesostructured metal catalysts can be prepared in one batch, whereas the conventional method requires at least two steps (i.e., synthesis of mesoporous materials + deposition of a catalytic metal).

In order to design mesostructured catalysts in a one-step procedure, it is important to understand the self-assembly of the templating agent, the silica source, and the metal ion used. In addition, the effects of synthesis variables such as the counteranion and temperature used in the assembly (specifically, in the case of a nonionic block copolymer as a templating agent) of mesostructured catalysts via the one-step procedure must be examined in detail. Because we adopted solution components that participate in the preparation of SBA-15, the self-assembly pathway of one-step mesostructured catalysts when a nickel salt is present can be tentatively expected to involve both an electrostatic attraction between $[S^0H^+]X^-$ and Ni^{2+}, and the complexation of Ni^{2+} with the polyethylene oxide (PEO) fragment in PEO_{20}-PPO_{70}-PEO_{20} [20–22]. Therefore, the assembly of mesostructured catalysts in one step probably is strongly dependent on the counteranion and the reaction temperature because the counteranion plays an important role in electrostatic interactions and the reaction temperature controls the volume of the PEO segment in the hydrophilic corona region. Hence, it is necessary to control both the counteranion and the temperature for the purpose of evaluating the self-assembly of the mesostructured catalysts via the one-step procedure.

In this study, we describe the preparation and characterization of mesostructured nickel catalysts, prepared via the one-step method and examined on the role of both the counteranion and the reaction temperature in the formation of the resulting mesostructured nickel catalysts by varying the counteranion (charge-matching) and by appropriately adjusting the reaction temperature. In addition, the physicochemical properties of the mesostructured catalysts are discussed in detail. The catalytic performance of the mesostructured nickel catalysts in the hydrodechlorination (HDC) of 1,1,2-trichloroethane (TCEa) into vinyl chloride monomer (VCM) was also tested.

2. Experimental

2.1. Synthesis of nickel catalysts (Ni-MH and Ni-MS) with ordered mesoporosity via a one-step procedure

A triblock copolymer [Pluronic P123 ($EO_{20}PO_{70}EO_{20}$, M_{av} = 5800), BASF] was used as a templating agent without further purification. Tetraethoxysilane (TEOS) was obtained from Aldrich. For the use in preparing mesostructured catalysts, nickel (II) sulfate hexahydrate ($NiSO_4{\cdot}6H_2O$) and nickel (II) nitrate hexahydrate ($Ni(NO_3)_2{\cdot}6H_2O$ were purchased from Junsei. Nickel catalysts with an ordered mesoporosity were typically prepared via a one step procedure in which the nickel precursor was dissolved before adding the TEOS (tetraethoxyorthosilicate). Briefly, for the preparation of Ni-MH, a total of 10 g of Pluronic P123, EO_{20}-PO_{70}-EO_{20}, was dissolved in 322 g of Millipore water. The resulting solution was mixed with 57 g of 2 M HCl. When the polymer was fully dissolved, the metal source ($Ni(NO_3)_2$) was added, followed by the addition of 21 g of TEOS. The molar ratio of nickel salt to TEOS was fixed at 1:2. The mixture was stirred at 35 °C for 20 h. After heating at 80 °C for 24 h, the resulting solid was isolated by filtration and washed. The solid product was calcined at 450 °C for 5 h in air. The final product was denoted as Ni-MH, where H is derived from HCl used as an acid source. For the preparation of Ni-MS (S indicates the use of H_2SO_4 as an acid), H_2SO_4, instead of HCl, was used as an acid source. The amount of H_2SO_4 was determined on the basis of H^+ (i.e., pH of the solutions was controlled so as to be the same). For a comparison of mesostructured catalysts prepared via a one-step procedure with that via conventional wetness impregnation (post-synthesis), Ni-SBA-15W was prepared. Before the preparation of Ni-SBA-15W, hexagonally ordered SBA-15 was prepared as described in the literature [1]. In a typical synthesis of Ni-SBA-15W, SBA-15 was treated with an aqueous solution of $Ni(NO_3)_2$ by the wetness impregnation method. After drying at 100 °C for 2 h, the solid product was calcined at 450 °C for 5 h in air.

2.2. The control of counteranion and reaction temperature

To investigate the role of the couteranion in the self assembly of Ni-MH and Ni-MS, two different acids (HCl, H_2SO_4) and nickel precursors [$NiSO_4$, $Ni(NO_3)_2$] were used. Several different reaction temperatures were tested to examine the effect of reaction temperature on the formation of Ni-MH and Ni-MS. It is well known that the synthesis of SBA-15 is usually carried out in two stages. The first reaction stage takes place at 35 °C. The second involves a thermal treatment (usually at 80 °C) where the aged gel is transferred to a teflon bottle and then heated for 24 h. In the present study, the temperature at the first reaction stage (before the aging step) was varied from 35, 42 to 50 °C. Except for the variation in the pre-stage temperature, the temperature of the second stage for Ni-MH and Ni-MS was fixed at 80 °C.

2.3. Characterization

N_2 adsorption/desorption experiments were carried out using a Micromeritics ASAP 2010 analyzer and pore size distributions were calculated using the Barrett–Joyner–Halenda (BJH) model on the adsorption branch. For the estimation of particle size and the morphology of the as-synthesized catalysts (Ni-MH and Ni-MS), SEM images of Ni-MH and Ni-MS were obtained using a Philips XL-20 scanning electron microscope. To confirm the presence of mesopore channels in Ni-MH, and Ni-MS, transmission electron microscopy (TEM) images were obtained on a JEOL JEM-2000EXII instrument operated at 200 kV. Small-angle X-ray scattering (SAXS) patterns were collected on a Bruker GADDS diffractometer using Cu Kα radiation at 40.0 kV and 45.0 mA. The nickel loading in each catalyst (Ni-MH and Ni-MS) was measured by inductively coupled plasma-atomic emission spectrometry (ICP-AES) on a Shimazu ICPS-1000IV instrument. The samples were reduced by temperature-programmed reduction (TPR) from room temperature to 900 °C (a ramping rate of 10 °C/min in a flow of 10% H_2 in nitrogen at atmospheric pressure). Powder X-ray diffraction (XRD) patterns of Ni-MH and Ni-MS were obtained with a Siemens D5000 diffractometer using nickel-filtered Cu Kα radiation. The crystalline phases in each catalyst were identified using the Joint Committee on Powder Diffraction Standards (JCPDS).

2.4. Hydrodechlorination of 1,1,2-trichloroethane

The hydrodechlorination of 1,1,2-trichloroethane to the vinyl chloride monomer was carried out in a continuous fixed bed reactor (i.d. = 1.0 cm) at atmospheric pressure. The prepared catalysts were charged in a tubular quartz reactor and activated in a stream of hydrogen (20 ml/min) and a helium carrier (20 ml/min) at 400 °C for 2 h and then reduced to the reaction temperature (300 °C). The reactant was fed by a Cole–Palmer syringe pump into the reactor. The exit flow from the reactor was passed through an alkali solution trap after the reaction, to absorb the HCl produced in the reaction. GC–MS and GC (HP 5890 gas chromatography) analysis were carried out to determine the product distribution in the HDC reaction.

3. Results and discussion

3.1. Characterization of as-made catalysts (Ni-MH and Ni-MS) prepared via a one-step procedure

N_2 isotherms for the one-step mesostructured catalysts (Ni-MH and Ni-MS) show irreversible type IV adsorption isotherms with an H1 hysteresis loop as defined by IUPAC (Fig. 1). The textural characteristics of Ni-MS and Ni-MH are summarized in Table 1. The pore size distributions (see inset in Fig. 1) are

Table 1
Textural characteristics of Ni-MS and Ni-MH

Catalysts	BET surface area (m^2/g)	Pore diameter(nm)	Pore volume (cm^3/g)	Nickel contents(%)
Ni-MS	812	7.9	0.90	1.8
Ni-MH	824	7.0	0.81	5.0
SBA-15	801	8.1	0.98	–
Ni-SBA-15W[a]	690	7.3	0.72	5.0

[a] This catalyst was synthesized using upper SBA-15 via incipient wetness impregnation.

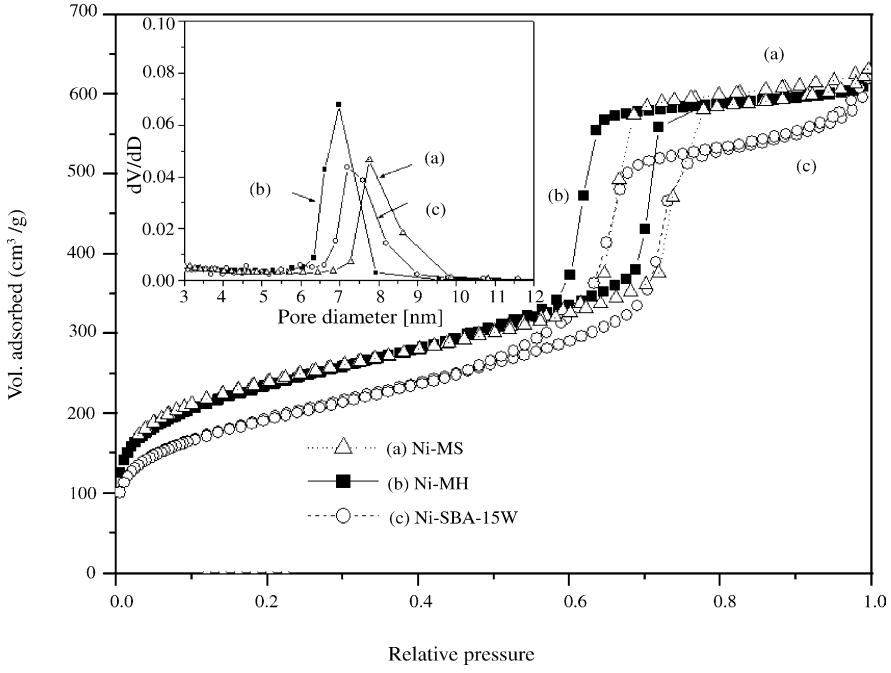

Fig. 1. N_2 adsorption/desorption isotherms of nitrogen at 77 K of: (a) Ni-MS; (b) Ni-MH; and (c) Ni-SBA-15W. (Inset) Pore size distribution of: (a) Ni-MS; (b) Ni-MH; and (c) Ni-SBA-15W. Pore size was calculated from the adsorption branch of the nitrogen adsorption/desorption isotherm using Barrett–Joyner–Halenda formula.

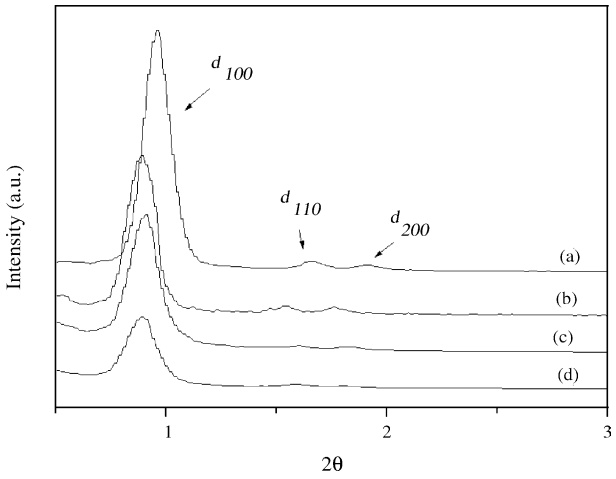

Fig. 2. Small-angle X-ray scattering patterns of: (a) Ni-MS; (b) bare SBA-15; (c) Ni-MH; and (d) Ni-SBA-15W. The data are shifted vertically for the sake of clarity.

narrow in the range of 6–8 nm (centered at 7.0 nm) for Ni-MH and 7–10 nm (centered at 7.9 nm) for Ni-MS. From Table 1, the physical properties of Ni-MS and Ni-MH are comparable to those of SBA-15, whereas the surface area, pore diameter and pore volume of Ni-SBA-15W are decreased as the result of the deposition of nickel oxide (NiO) via the wetness impregnation method. Direct comparisons of the pore properties of SBA-15 with Ni-SBA-15W such as surface area and pore size are possible because Ni-SBA-15W was prepared using a post-synthetic method. The pore sizes of Ni-MH and Ni-MS were slightly smaller than that of SBA-15. It has been reported that the crystallization of a silica-surfactant assembly, in the presence of a salt, would be expected to favor the formation of an SBA-15 framework having a reduced pore size [23]. The pore size of Ni-MS (the amount of nickel is 1.8 wt.%, where wt. indicates the weight percentage) is larger than that of Ni-MH (the amount of nickel is 5 wt.%) by ca. 0.9 nm due to the difference in the amount of deposited NiO. The SAXS patterns for the prepared catalysts are shown in Fig. 2. The SAXS patterns of Ni-MH and Ni-MS show a strong (1 0 0) reflection at 0.91° (2θ value). Two additional high order peaks for both (1 1 0) and (2 0 0) planes with lower intensities with 2θ values of 1.5°–1.9° were also observed for Ni-MH and Ni-MS. This indicates that both Ni-MS and Ni-MH also have a highly ordered pore arrangement and the space group of Ni-MH and Ni-MS belongs to *p*6*mm*, which is characteristic of a hexagonal pore structure. The decrease in (1 0 0) intensity for Ni-SBA-15W compared with SBA-15 provides that NiO is deposited inside the mesopore channels since the attachment of materials to the surface of the mesopore channels tends to reduce the scattering power (or scattering contrast) of the amorphous silicate wall [24,25]. The XRD pattern (Fig. 3A) of Ni-MH shows peaks at 2θ = 37°, 43°, 62°, 72°, and 79°, which are characteristic of NiO plane indices of (1 0 1), (1 0 2), (1 1 0), (1 1 3) and (2 0 2), respectively. In the XRD pattern of Ni-MS, the intensities of each peak decrease dramatically, indicative of a reduction in the size of NiO because peak sharpness and intensity are proportional to metal size. The size of NiO in Ni-MH, as estimated from the Sherrer equation, is about 4 nm, which is

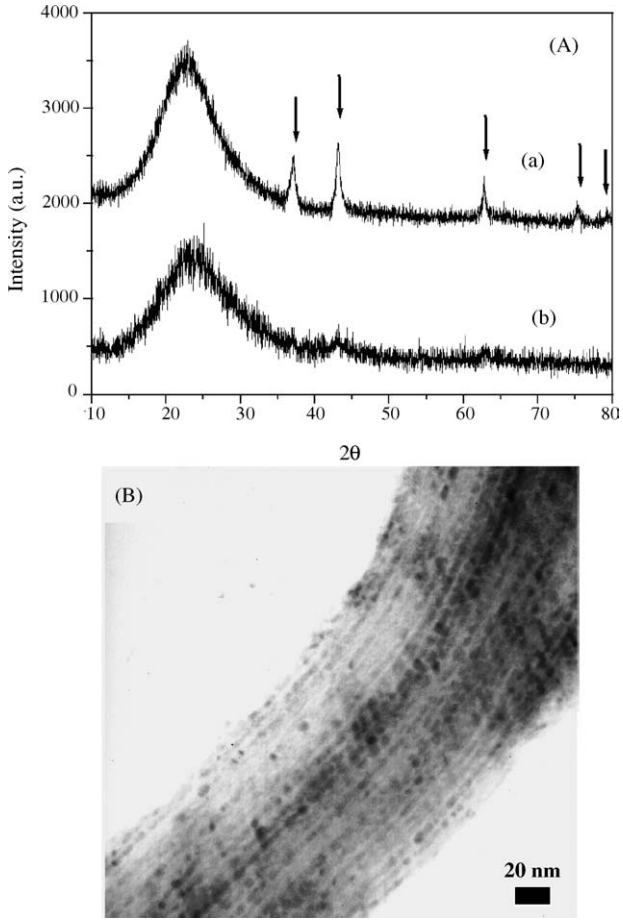

Fig. 3. (A) X-ray diffraction patterns of: (a) Ni-MH and (b) Ni-MS. The data are shifted vertically for the sake of clarity. (B) TEM image of Ni-MH ($Ni(NO_3)_2$ as nickel source).

in good agreement with the TEM observations (Fig. 3B). From the extensive investigations of TEM and XRD analyses of Ni-MH and Ni-MS, no NiO as a separate crystallite phase (i.e., unsupported NiO) could be detected. The TPR profiles (Fig. 4) of Ni-MS and Ni-MH show typical peaks (between 327 and

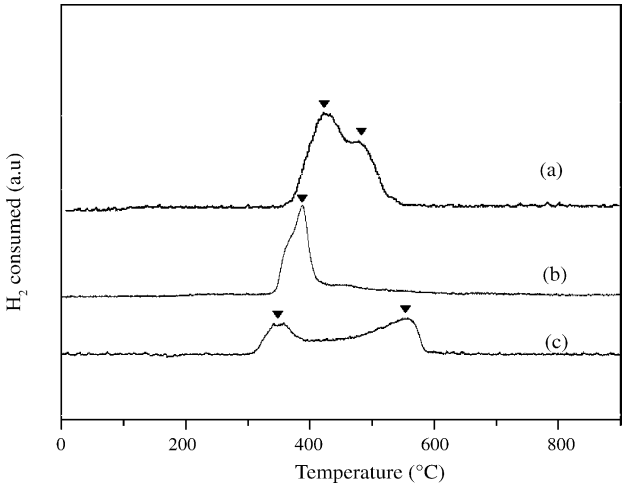

Fig. 4. Temperature programmed reduction (TPR) profile of: (a) Ni-MS; (b) Ni-MH; and (c) Ni-SBA-15W.

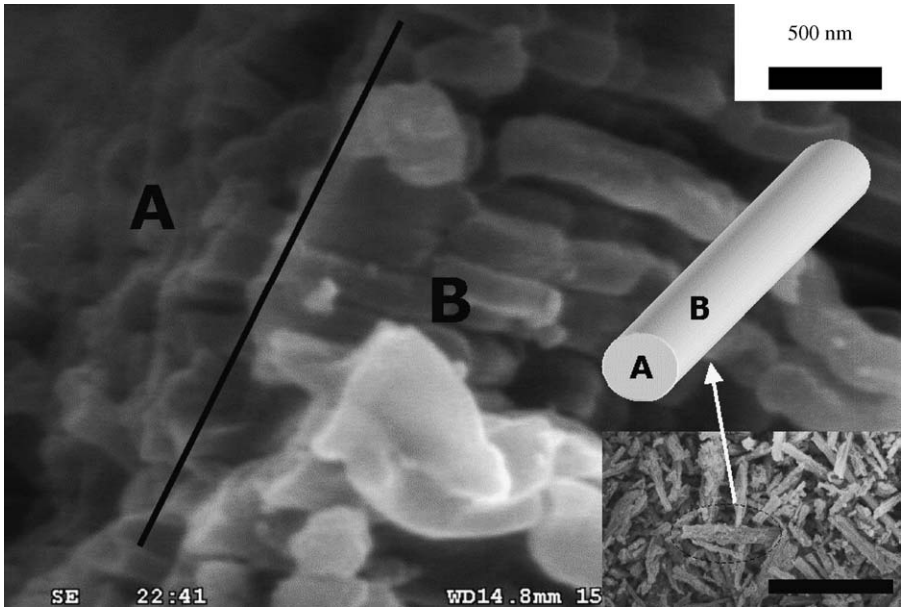

Fig. 5. SEM image of Ni-MS at the edge of the aggregates. (Inset) SEM image of Ni-MS with different magnification (scale bar of inset corresponds to 50 μm).

427 °C) for reduced NiO species supported on SiO_2, whereas two distinct reduction peaks are observed in the case of Ni-SBA-15W. The two reduction profiles of Ni-SBA-15W are tentatively assigned to the two collections of crystallites of different particle size (separate crystallite + embedded crystallite in the mesopore channel of the support). Fig. 5 shows that both Ni-MS and Ni-MH consist of numerous rod-like particles with relatively uniform sizes of 1 μm, which are aggregated into a macrostructure (see inset in Fig. 5). The strongly aggregated macrostructure is similar to the cylindrical shape. Fig. 5 also shows that the edge (A side) of aggregates of Ni-MS and Ni-MH is uniform on the sub-micron scale. For the self assembly of a block copolymer and a metal ion, it has been reported that transition metal ions such as Cu^{2+} and Ni^{2+} form crown-ether-type complexes with polymeric PEO and PPO units, where the multivalent metal species (M^{n+}) preferentially associate with the hydrophilic PEO moieties because of their different binding affinities for PEO and PPO [26]. When the synthesis mixture contains metal ions, the modified pathway can now be denoted as $N^0[(M^{n+} + H^+)X^-]I^+$ where M^{n+} is the modifying ion, which results in branched mesopore channels. However, in the present study, based on the TEM images of Ni-MS and Ni-MH, no branched mesoporous structure formation was observed.

3.2. The effect of the counteranion

A counteranion is more or less hydrated in the surfactant solution. More strongly hydrated ions, in general, have larger ionic radii and bind less tightly to the head group of the surfactant. It is well known that the aggregation number or the ionic radii decreases in the following order [27,28]: $\frac{1}{2}SO_4^{2-} > Cl^- > Br^- > NO_3^-$. It is assumed that large anions contribute to the partial reduction in electrostatic repulsion between the positively charged polyethylene oxide (PEO) branch and nickel ions. Furthermore, it would be expected that large and divalent anion attracts metal ions more effectively than small, monovalent anions from the standpoint of electrostatic interactions. Moreover, from order of Gibbs free energy of formation [$NiSO_4$ ($-790\,kJ\,mol^{-1}$) ≪ $NiCl_2$ ($-307.9\,kJ\,mol^{-1}$) < $Ni(NO_3)_2$ ($-268.5\,kJ\,mol^{-1}$)] [29], SO_4^{2-} would be expected to interact with Ni^{2+} more strongly. Therefore, an alternate acid source (H_2SO_4) was selected to investigate the effect of the counteranion (SO_4^{2-}) on the amount of metal loading. In spite of changing the acid source to H_2SO_4, which is divalent and has a larger ionic radius, no increase in the amount of metal loading was observed. This phenomenon can be attributed to the nature of the ionization of H_2SO_4. It is well known that H_2SO_4 undergoes ionization in two steps (pK_a values for the 1st and 2nd step are −2 and 2) in aqueous solution. The 1st step is completely irreversible, whereas the 2nd deprotonation is quite reversible. Therefore, it can be inferred that the monovalent and smaller ionic radii of HSO_4^- compared to SO_4^{2-} acts as an intermediating anion. It was observed, however, that a different counteranion by changing the nickel salt (changing from $Ni(NO_3)_2$ to $NiSO_4$) leads to a significant change in the amount of nickel loading. The amount of nickel loaded on Ni-MH is slightly increased from 5 wt.% ($Ni(NO_3)_2$ as the nickel salt) to 5.5 wt.% ($NiSO_4$ as the nickel salt). However, the amount of nickel loaded on Ni-MS is increased much more from 1.8 wt.% ($Ni(NO_3)_2$ as the nickel salt) to 3.3 wt.% ($NiSO_4$ as the nickel salt). Fig. 6 shows that the deposition of NiO in Ni-MS and Ni-MH prepared using $NiSO_4$ as the nickel salt clearly occurs (Fig. 6C). Therefore, it can be concluded that altering the counteranion to the larger, divalent SO_4^{2-} results in an increased nickel loading for both Ni-MH and Ni-MS and that this is the result of enhanced electrostatic interactions. However, the differences in the extent of increase in the amount of nickel loaded on Ni-MH and Ni-MS suggest that the self-assembly routes for

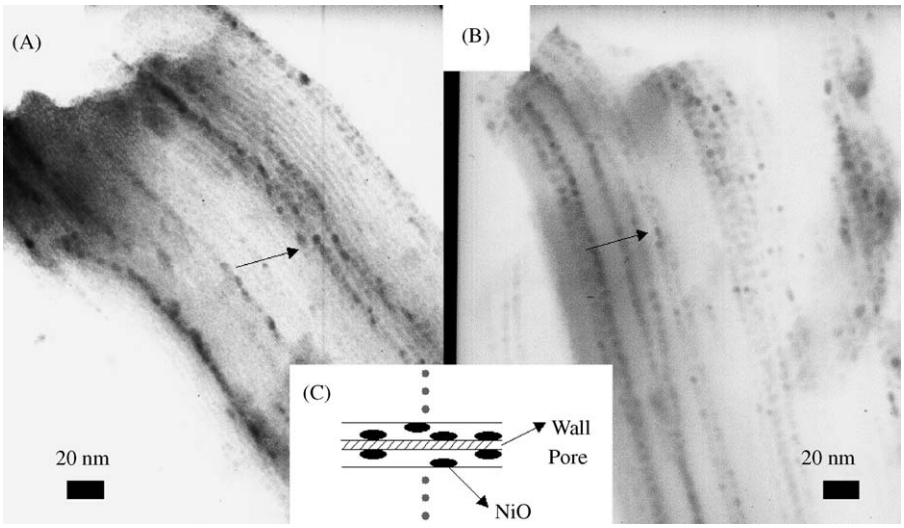

Fig. 6. TEM images of (A) Ni-MH and (B) Ni-MS prepared using $NiSO_4$ as nickel source (synthesis temperature 35 °C). (C) Schematic diagram of NiO located on the surface of the mesopore channel.

Ni-MH and Ni-MS are different. It would be expected that the driving force for the assembly between metal ion (Ni^{2+}) and the templating agent (PEO_{20}-PPO_{70}-PEO_{20}) in the one step procedure involves electrostatic interactions through $S^0H^+X^-(I^+$ or $M^{n+})$, in which the inorganic precursor (I^+) and nickel ion acts as a competing cation and complexation through S^0M^{n+} [26], in which a PEO fragment in S^0 appears to play a critical role [30]. The fact that the amount of nickel loaded on Ni-MH (HCl as the acid source) is independent of the choice of nickel salt and that chloride anion (Cl^-) plays a vital role in the interaction between the PEO branch and the transition metal ion [26], in turn, suggests that the assembly of Ni-MH occurs dominantly through complexation between PEO and nickel ions. It can be also inferred that the self assembly of Ni-MS follows a dominantly electrostatic pathway, based on the fact that changing the nickel salt results in a drastic change in the amount of nickel loaded on Ni-MS. Small anions contribute to the partial reduction in the intramolecular electrostatic repulsion between the positively charged repeating units (S^0H^+) more effectively than larger anions. Hence, it is understandable that the larger anion, SO_4^{2-}, hinders the formation of a crown-ether-type conformation of the PEO fragment due to the stiffness of positively charged PEO chain (in strongly acidic solution), similar to a polyelectrolyte.

3.3. The effect of synthesis temperature

If the assumption that the prevailing self assembly routes between Ni^{2+} and a block copolymer are electrostatic for Ni-MS and involve complexation by PEO for Ni-MH (aided by Cl^- anion) is operating, it would be expected that the amount of nickel loading should be strongly affected by the synthesis temperature, since the distribution of PEO within the micellar structure of PEO_x-PPO_y-PEO_x is critically dependent on temperature [31]. It is well known that in a typical synthesis of SBA-15, a low temperature step is followed by a high temperature hydrothermal stage (aging step). In a recent paper by Ruthstein et al. [32,33] on the formation of SBA-15 using EPR spectroscopy, it was reported that after 20 min of reaction, the EO chains have a different environment, which can be attributed to their being located either in the micellar corona or in the micropores respectively. In addition, they found that the hexagonal structure appears 2 h after the beginning of the self-assembly of the surfactant and TEOS, as evidenced by EPR spectroscopy experiments. In other words, the assembly of the surfactant and the silica precursor is complete within a few hrs. Hence, it would be expected that control of the reaction temperature in the initial stage before aging (temperature of 80 °C) would be a crucial determinant of the amount of metal loaded and the pore structure in mesostructured catalysts produced via the one-step procedure. When the reaction temperature in the initial stage is increased from 35 to 50 °C, a decrease in the amount of metal loading of both Ni-MH and Ni-MS is observed. The amount of nickel loaded on the Ni-MS was decreased slightly from 3.3 (at 35 °C) to 3.1 wt.% (at 50 °C). However, the amount of nickel loaded on the Ni-MH decreased significantly from 5 (at 35 °C) to 1.9 wt.% (at 50 °C). This result (strong temperature-dependent behavior of the nickel content in Ni-MH) is in agreement with the previous assumption. Such a decrease in the amount of nickel loading for Ni-MH is closely related to the micellar structure, which varies with temperature. In general, as the temperature of a micellar solution increases, the PEO blocks become hydrophobic, resulting in an increased volume of hydrophobic domain. This indicates that the sites (PEO fragment) available for interaction with Ni^{2+} are diminished. Therefore, it is understandable that the amount of nickel loaded on Ni-MH is inversely proportional to the temperature.

3.4. Morphology control of Ni-MH and Ni-MS

When the pre-stage temperature was varied, the particle morphologies were found to be highly sensitive to the synthesis temperature used, even in a narrow region (35–50 °C). It has

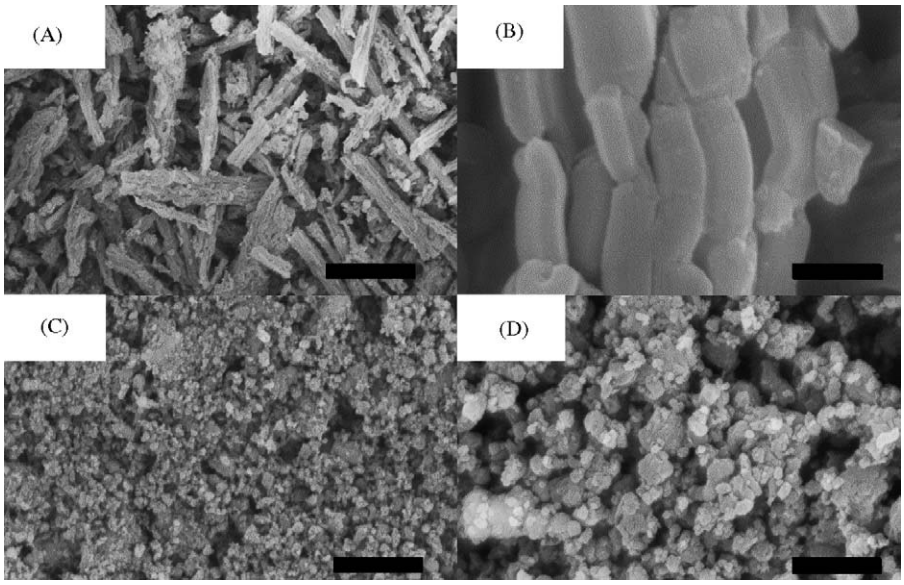

Fig. 7. Representative scanning electron micrographs (SEM) of: (A) Ni-MH at 35 °C; and with magnification (B). SEM image of (C) Ni-MH synthesized at 50 °C; and with magnification (D). Scale bars correspond to 25, 1, 10, and 2.5 μm, respectively.

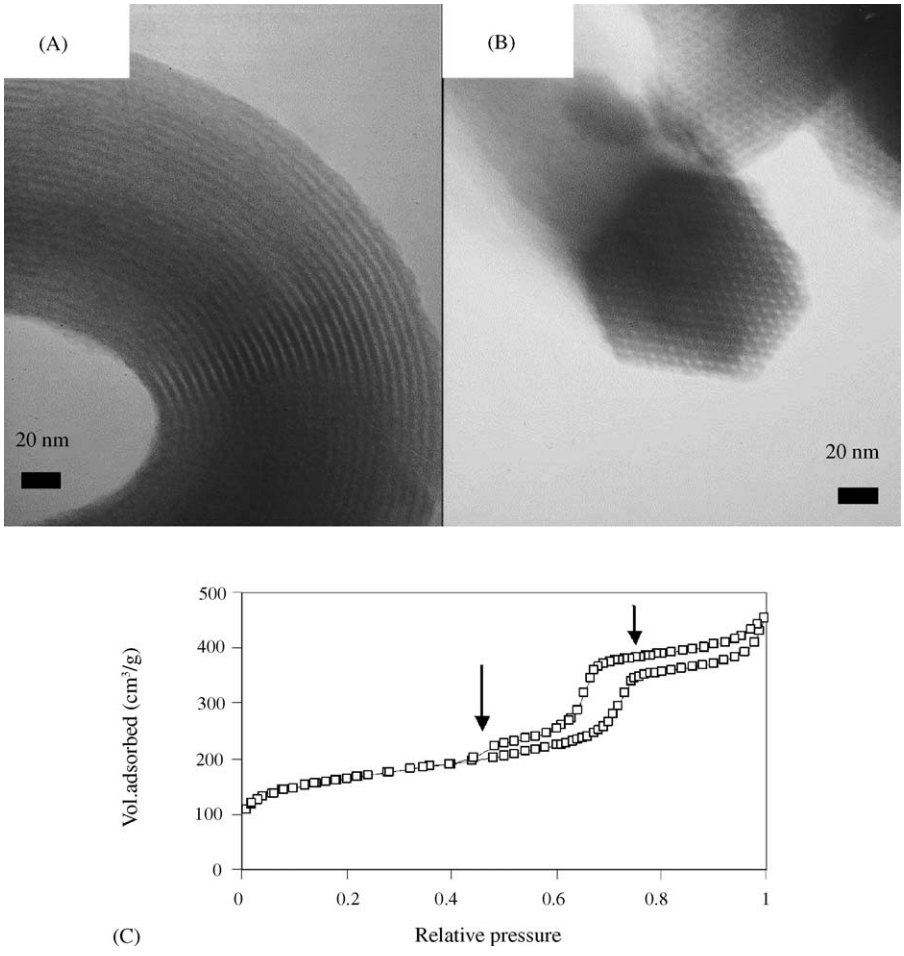

Fig. 8. TEM images of Ni-MH at: (A) 50 °C and (B) TEM image of (A) at a different zone axis. The scale bars correspond to 20 nm. (C) N_2 adsorption/desorption isotherm of nitrogen at 77 K corresponds to Ni-MS prepared at 50 °C. Arrows are indicative of plugged pore structures.

been reported that the shape of mesoporous silica powder particles is controlled by several complex factors including the condensation rate of the silica species, the shape of the surfactant micelles, the concentration of inorganic salts, and the rate of stirring [34–36]. Fig. 7 shows the transitions in the morphology of Ni-MH as a function of reaction temperature. As the reaction temperature increases, uniform spherical particles (rather than rod-like shape) are produced. The morphologies of both Ni-MH and Ni-MS prepared via the one step procedure can be manipulated so as to produce either rod-like or spherical particles. The control of catalyst morphology is important, because in actual industrial applications, particle packing, which mainly depends on particle morphology, plays a crucial role in catalytic performance.

TEM images reveal that the increase in reaction temperature results in a more curved mesopore channel. Fig. 8A shows that representative U-shaped mesopores are present in both Ni-MS.and Ni-MH prepared at 50 °C. Nonetheless, the pores are still hexagonally arranged as would be expected for a material synthesized at 35 °C (Fig. 8B). It has been suggested that a slower condensation rate (such as that for TEOS) yields a more curved rope-like SBA-15 morphology [37]. These results indicate that the control of the pre-stage reaction temperature affects the pore curvature of Ni-MH and Ni-MS on a meso-scale. The major difference between one-step mesostructured catalysts synthesized at lower temperature (35 °C) and higher temperature (42 °C and 50 °C) in N_2 adsorption/desorption isotherms (Fig. 8C) is that the hysteresis loop does not end after capillary actions and capillary evaporation occurs in two-step processes that feature the second desorption branch formed at a lower relative pressure. It has been reported that this type of two-step branched desorption isotherm arises from plugged mesopores [38,39].

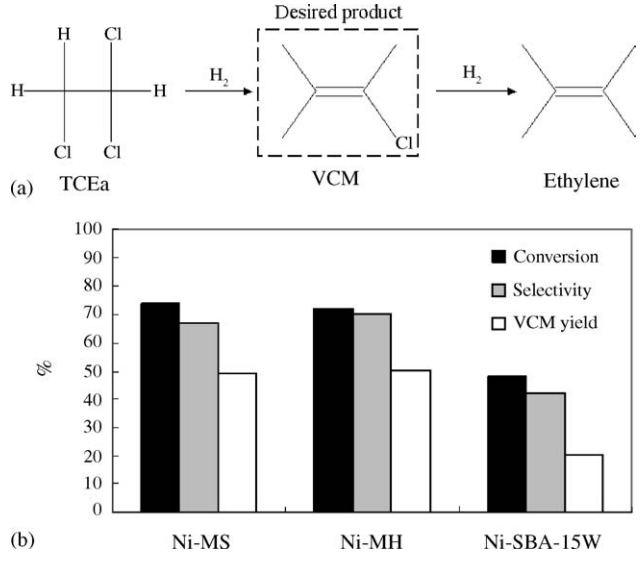

Fig. 9. Proposed scheme: (a) for the selective hydrodechlorination of 1,1,2-TCEa to VCM over nickel catalysts[28a] (not drawn to scale) and representative catalytic performances and (b) of Ni-MS, Ni-MH, and Ni-SBA-15W after 6 h of use.

3.5. Catalytic activity for hydrodechlorination of 1,1,2-trichloroethane

As-synthesized mesostructured catalysts (Ni-MH and Ni-MS) were tested in the hydrodechlorination of 1,1,2-trichloroethane as a model catalytic application. In such a catalytic system (Fig. 9a), the yield of the more useful unsaturated hydrocarbon serves as a measure of catalytic performance [40,41]. As shown in Fig. 9b, Ni-MS and Ni-MH show much higher catalytic acitivities than the mesostructured catalyst prepared by multi-step wetness impregnation (Ni-SBA-15W). Furthermore, the yields of VCM, the most desirable product (because of its recyclable nature) for both Ni-MS and Ni-MH are also higher than Ni-SBA-15W by over 25% (Ni-MS). It should be noted that the trend is still maintained after 10 h (time on stream). It should be noted that catalytic performance such as VCM selectivity, yield, and a steady reaction activity are dependent on a variety of variables including the status of the adsorption sites, pore connectivity, and the ensemble effect. Hence, in order to assess the catalytic activities of Ni-MS and Ni-MH in the HDC reaction more specifically, further studies are currently underway.

4. Conclusions

A facile and rapid synthesis using different acid sources including nickel salts and initial stage reaction temperatures for the preparation of mesostructured catalysts is described. Ni-MH and Ni-MS were prepared using different acid sources (HCl or H_2SO_4) and nickel precursors ($NiSO_4$ or $Ni(NO_3)_2$), respectively. The results show that both Ni-MH and Ni-MS have acceptable structural characteristics such as alignment (space group, *p*6*mm*) and uniform mesoscopic channels except that the shrinkage (∼1 nm) of the pore size of Ni-MH occurred and the size of the nickel particles in Ni-MS is smaller than in Ni-MH. The deposition of NiO in Ni-MH was found to occur along the mesopore channel. Changing the nickel precursor from $Ni(NO_3)_2$ to $NiSO_4$ results in an increase in the amount of nickel loaded on both Ni-MS and Ni-MH. However, we conclude that the morphologies of the mesostructured catalysts, prepared in one step are less dependent on the counteranion present. The increase in nickel content can be tentatively explained by enhanced electrostatic interactions between nickel ion (Ni^{2+}) and the counteranion in the case of $NiSO_4$ as a nickel salt, which is in a good agreement with thermodynamic data (the Gibbs free energy of the formation). The dependence of both counteranion and temperature on nickel loading can be clearly understood by assuming that the self-assembly of Ni-MH and Ni-MS probably involves an electrostatic pathway and complexation between a polyethylene oxide branch in P123 and Ni^{2+}. The findings herein suggest that the prevailing self-assembly route involves electrostatic interactions for Ni-MS, and coordination by PEO for Ni-MH. The morphologies of the mesostructured catalysts prepared in one step can be manipulated so as to produce uniform rod-like forms or uniform spherical particles by varying the reaction temperature appropriately. As the reaction temperature increases, both Ni-MH and Ni-MS

appears to adopt a more curved shape from both the meso and macroscopic view. In addition, the findings herein also suggest that mesostructured catalysts, Ni-MH and Ni-MS can be successfully used in hydrodechlorination reactions. We expect that these mesostructured catalysts prepared via a one-step procedure will have practical importance because a one-step method could increase the economic feasibility of producing ordered mesoporous materials for further applications.

Acknowledgement

We are grateful to the Eco-Technopia-21 Project of Ministry of Environment, Korea, for financial support, and this research was conducted through the Engineering Research Institute (ERI) at Seoul National University.

Appendix A. Supplementary data

Supplementary data associated with this article can be found, in the online version, at doi:10.1016/j.molcata.2005.09.003.

References

[1] D. Zhao, J. Feng, Q. Huo, N. Melosh, G.H. Fredrickson, B.F. Chmelka, G.D. Stucky, Science 279 (1998) 548.
[2] R.T. Yang, T.J. Pinnavaia, W. Li, W. Zhang, J. Catal. 172 (1997) 488.
[3] D. Eliche-Quesada, J. Mérida-Robles, P. Maireles-Torres, E. Rodríguez-Castellón, A. Jiménez-López, Langmuir 19 (2003) 4985.
[4] R.J.P. Corriu, E. Lancelle-Beltran, A. Mehdi, C. Reyé, S. Brandès, R. Guilard, J. Mater. Chem. 12 (2002) 1355.
[5] D. Margolese, J.A. Melero, S.C. Christiansen, B.F. Chmelka, G.D. Stucky, Chem. Mater. 12 (2000) 2448.
[6] W.M. Van Rhijn, D.E. De Vos, B.F. Sels, W.D. Bossaert, P.A. Jacobs, Chem. Commun. (1998) 317.
[7] Y.S. Cho, J.C. Park, B. Lee, Y. Kim, J. Yi, Catal. Lett. 81 (2002) 89.
[8] Y. Park, T. Kang, Y.S. Cho, J.C. Park, J. Yi, Stud. Surf. Sci. Catal. 146 (2003) 637.
[9] K. Mukhopadhyay, B.R. Sarkar, R.V. Chaudhari, J. Am. Chem. Soc. 124 (2002) 9692.
[10] T. Kang, Y. Park, J. Yi, Ind. Eng. Chem. Res. 43 (2004) 1478.
[11] S. Dai, M.C. Burleigh, Y.S. Shin, C.C. Morrow, C.E. Barnes, Z.L. Xue, Angew. Chem. Int. Ed. 38 (1999) 1235.
[12] T. Kang, Y. Park, K. Choi, J.S. Lee, J. Yi, J. Mater. Chem. 14 (2004) 1043.
[13] Y. Kim, C. Kim, I. Choi, S. Rengaraj, J. Yi, Environ. Sci. Technol. 38 (2004) 924.
[14] H.S. Zhou, H. Sasabe, I. Honma, J. Mater. Chem. 8 (1998) 515.
[15] M. Kruk, R. Ryoo, S.H. Joo, M. Jaroniec, J. Phys. Chem. B 104 (2000) 7960.
[16] M. Kruk, M. Jaroniec, S.H. Joo, R. Ryoo, J. Phys. Chem. B 107 (2003) 2205.
[17] Z. Kónya, V.F. Puntes, I. Kiricsi, J. Zhu, J.W. Ager III, M.K. Ko, H. Frei, P. Alivisatos, G.A. Somorjai, Chem. Mater. 15 (2003) 1242.
[18] M. Hartmann, A. Vinu, Langmuir 18 (2002) 8010.
[19] K. Cassiers, T. Linssen, M. Mathieu, M. Benjelloun, K. Schrijnemakers, P. Van Der Voort, P. Cool, E.F. Vansant, Chem. Mater. 14 (2002) 2317.
[20] Q. Huo, D.I. Margolese, U. Ciesla, D.G. Demuth, P. Feng, T.E. Gier, P. Sieger, A. Firouzi, B.F. Chmelka, F. Schuth, G.D. Stucky, Chem. Mater. 6 (1994) 1176.
[21] J.Y. Ying, C.P. Mehnert, M.S. Wong, Angew. Chem. Int. Ed. 38 (1999) 56.
[22] D. Zhao, Q. Huo, J. Feng, B.F. Chmelka, G.D. Stucky, J. Am. Chem. Soc. 120 (1998) 6024.
[23] B.L. Newalkar, S. Komarneni, Chem. Mater. 13 (2001) 4573.
[24] B. Marler, U. Oberhagemann, S. Vortmann, H. Gies, Micropor. Mater. 6 (1996) 375.
[25] L. Mercier, T.J. Pinnavaia, Environ. Sci. Technol. 32 (1998) 2749.
[26] Z. Konya, J. Zhu, A. Szegedi, I. Kiricsi, P. Alivisatos, G.A. Somorjai, Chem. Commun. (2003) 314.
[27] S. Che, S. Lim, M. Kaneda, H. Yoshitake, O. Terasaki, T. Tatsumi, J. Am. Chem. Soc. 124 (2002) 13962.
[28] L. Gaillon, J. Lelievre, R. Gaboriaud, J. Colloid Interface Sci. 213 (1999) 287.
[29] CRC Handbook of Chemistry and Physics, 77th ed., CRC Press, London, 1996.
[34] D. Zhao, J. Sun, Q. Li, G.D. Stucky, Chem. Mater. 12 (2000) 275.
[30] W. Zhang, B. Glomski, T.R. Pauly, T.J. Pinnavaia, Chem. Commun. (1999) 1803.
[31] P. Kipkemboi, A. Fodgen, V. Alfredsson, K. Flodstrom, Langmuir 17 (2001) 5398.
[32] S. Ruthstein, V. Frydman, S. Kababya, M. Landau, D. Goldfarb, J. Phys. Chem. B 107 (2003) 1739.
[33] S. Ruthstein, V. Frydman, D. Goldfarb, J. Phys. Chem. B 108 (2004) 9016.
[35] H. Yang, G. Vouk, N. Coombs, I. Sokolov, G.A. Ozin, J. Mater. Chem. 8 (1998) 743.
[36] S. Shio, A. Kimura, M. Yamaguchi, K. Yoshida, K. Kuroda, Chem. Commun. (1998) 2461.
[37] A.H. Janssen, P. Van Der Voort, A.J. Koster, K.P. De Jong, Chem. Commun. (2002) 1632.
[38] J. Lee, Y. Park, P. Kim, H. Kim, J. Yi, J. Mater. Chem. 14 (2004) 1050.
[39] P. Van Der Voort, P.I. Ravikovitch, A.V. Neimark, M. Benjelloun, E. Van Bavel, K.P. De Jong, B.M. Weckhuysen, E.F. Vansant, Stud. Surf. Sci. Catal. 141 (2002) 45.
[40] Y. Choi, W. Lee, J. Mol. Catal. A 174 (2001) 193.
[41] P. Kim, Y. Kim, H. Kim, I.K. Song, J. Yi, J. Mol. Catal. A 219 (2004) 87.